PHYSICAL REVIEW A **78**, 010902(R) (2008)

Quantum reflection of helium atom beams from a microstructured grating

Bum Suk Zhao,[1] Stephan A. Schulz,[2] Samuel A. Meek,[1] Gerard Meijer,[1] and Wieland Schöllkopf[1,*]
[1]*Fritz-Haber-Institut der Max-Planck-Gesellschaft, Faradayweg 4-6, 14195 Berlin, Germany*
[2]*Institut für Quanteninformationsverarbeitung, Universität Ulm, Albert-Einstein-Allee 11, 89069 Ulm, Germany*
(Received 31 January 2008; revised manuscript received 11 April 2008; published 29 July 2008)

We observe high-resolution diffraction patterns of a thermal-energy helium atom beam reflected from a microstructured surface grating at grazing incidence. The grating consists of 10-μm-wide Cr strips patterned on a quartz substrate and has a periodicity of 20 μm. Fully resolved diffraction peaks up to the seventh order are observed at grazing angles up to 20 mrad. With changes in de Broglie wavelength or grazing angle the relative diffraction intensities show significant variations which shed light on the nature of the atom-surface interaction potential. The observations are explained in terms of quantum reflection at the long-range attractive Casimir–van der Waals potential.

DOI: 10.1103/PhysRevA.78.010902 PACS number(s): 34.35.+a, 03.75.Be, 37.25.+k, 68.49.Bc

Optical elements, such as mirrors and coherent beam splitters for matter waves, are prerequisites for atom and molecule interferometry. Both gratings formed by laser light and material gratings have been employed in Ramsey-Bordé and Mach-Zehnder matter-wave interferometers, respectively [1]. As the de Broglie wavelengths of atoms and molecules at thermal energies are typically $\leqslant$0.1 nm, free-standing material transmission gratings of submicrometer periodicity had to be used in interferometers for beams of Na atoms [2], dimers [3], and C_{60} fullerenes [4,5]. In addition, diffraction by a 100-nm-period transmission grating was applied to quantitatively determine long-range atom-surface van der Waals potentials [6,7] and to investigate small He clusters [8]. Those gratings are, however, difficult to make, expensive, and fragile. Shimizu and co-workers demonstrated diffraction of ultracold atoms, released from a magneto-optical trap, by a 2-mm-period surface grating with reflective strips consisting of parallel 100-nm-wide ridges [9]. Most recently, partially resolved diffraction peaks of thermal beams of metastable rare-gas atoms reflecting from a 2-μm-period surface grating were reported [10].

Here, we present diffraction patterns of He atom beams that are coherently reflected from a homemade 20-μm-period surface grating under grazing incidence. For incident grazing angles in the milliradian range, the resulting diffraction angles are of the same order of magnitude as the ones observed with a 100-nm-period transmission grating at normal incidence [11]. The projection of the grating period along the incident beam direction yields an effective grating period in the submicrometer range. Yet a 20-μm-period surface grating can readily be made out of a variety of materials using standard lithographic techniques. Unlike for He atom beam scattering from smooth crystalline surfaces [12], ultrahigh vacuum and *in situ* surface preparation are not needed, but coherent reflection is achieved with a microscopically rough surface.

We present evidence for the underlying coherent reflection mechanism being *quantum reflection* at the attractive long-range branch of the atom-surface interaction [13]. Quantum reflection from a solid surface was observed recently with ultracold metastable Ne [14] and He atoms [15], with a Bose-Einstein condensate [16], and with a ^{3}He atom beam [17]. It was described theoretically in terms of the long-range Casimir–van der Waals atom-surface potential [13]. Furthermore, Shimizu and co-workers reported diffraction of ultracold metastable He atoms quantum-reflected from ridged surfaces [9,18].

In the apparatus[1] a helium atom beam is formed by free-jet expansion of pure ^{4}He gas from a source cell (stagnation temperature T_0 and pressure P_0) through a 5-μm-diameter orifice into high vacuum. As indicated in Fig. 1 the beam is collimated by two narrow slits, each 20 μm wide, located 15 and 115 cm downstream from the source. A third 25-μm-wide detector-entrance slit, located 38 cm downstream from the grating, limits the angular width of the atomic beam to a full width at half maximum of 130 μrad. The detector is an electron-impact ionization mass spectrometer that can be rotated precisely around the angle θ indicated in Fig. 1. The microstructured reflection grating is positioned at the intersection of the horizontal atom beam axis and the vertical detector pivot axis such that the incident atom beam impinges under grazing incidence (incident grazing angle $\theta_{\mathrm{in}} \leqslant 20$ mrad), with the grating lines oriented parallel to the pivot axis. The diffraction pattern is measured by rotating the detector around θ and measuring the mass spectrometer signal at each angular position.

The reflection grating consists of a 56-mm-long microstructured array of 110-nm-thick, 10-μm-wide, and 5-mm-long parallel chromium strips on a flat quartz substrate. It was made from a commercial chromium mask blank by electron-beam lithography. As shown in the inset of Fig. 1, the center-to-center distance of the strips, and thereby the period d, is 20 μm. Given this geometry, the quartz surface between the strips is completely shadowed by the strips for all the incidence angles used. We expect a chromium oxide surface to have formed while the grating was exposed to air before mounting it in the apparatus where the ambient vacuum is about 8×10^{-7} mbar. No *in situ* surface preparation was done.

*wschoell@fhi-berlin.mpg.de

[1]This apparatus was built at the Max-Planck-Institut für Strömungsforschung in Göttingen, Germany.

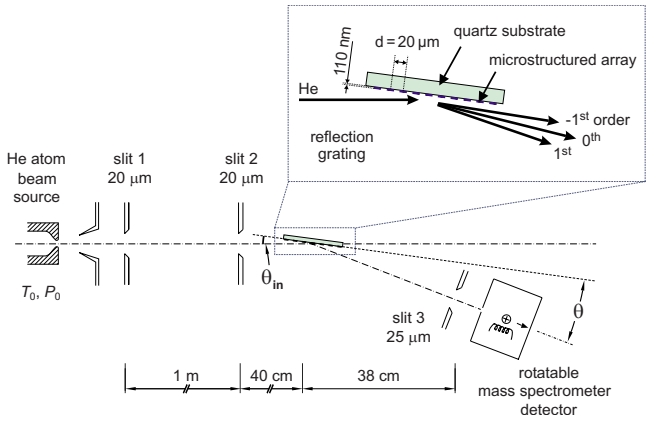

FIG. 1. (Color online) Scheme of the experimental setup. Diffraction patterns are recorded by scanning the detection angle θ, which is defined with respect to the reflection-grating surface plane. The inset in the upper right shows an enlargement of the grating indicating the directions of the zeroth- and first-order diffraction beams.

Figure 2(a) shows a series of diffraction patterns measured at constant source conditions of $T_0=20$ K and $P_0=6$ bar corresponding to a de Broglie wavelength of $\lambda=2.2$ Å. The incident grazing angle θ_{in} was varied between 3 and 15 mrad. The most intense peak in each diffraction pattern is attributed to the specular reflection (zeroth-diffraction-order peak), for which the detection angle is equal to the incident grazing angle. The intensity of the specular peak decreases continuously from about 600 counts/s at $\theta_{in}=3.1$ mrad to only 13 counts/s at $\theta_{in}=15.2$ mrad. At $\theta_{in}=3.1$ mrad at least seven positive-order diffraction peaks can be seen at angles larger than the specular angle (diffraction "away from the surface"), while no negative diffraction-order peak is present. With increasing incident grazing angle, negative-order diffraction peaks appear successively.

The diffraction angles ϑ_n are defined as the angular separation between the nth- and zeroth-diffraction-order peaks, $\vartheta_n=\theta_n-\theta_0$, and are analyzed in Fig. 2(b). It is straightforward to calculate the diffraction angles using the grating equation $\cos(\theta_{in})-\cos(\theta_n)=n\lambda/d$ [19]. Here θ_n is the angle (with respect to the grating surface plane) of the nth-diffraction-order peak, and λ is the de Broglie wavelength. The calculated diffraction angles [lines in Fig. 2(b)] agree with the observed ones within the experimental error, thereby unambiguously confirming the interpretation of the peaks as grating-diffraction peaks. Note that with decreasing incidence angle the negative-order diffraction peaks disappear successively when the cutoff condition $\vartheta_n<-\theta_{in}$ is met, i.e., when the peak is diffracted "into the surface." This regime is indicated by the gray-shaded region in Fig. 2(b).

The relative diffraction peak intensities change significantly with incident grazing angle. For instance, for $\theta_{in}=3.1$ mrad even- and odd-order peaks have similar heights falling off almost monotonically with increasing diffraction order. With increasing incident grazing angle, however, the positive-even-order diffraction peaks tend to disappear. Moreover, a distinct peak-height variation can be seen for the

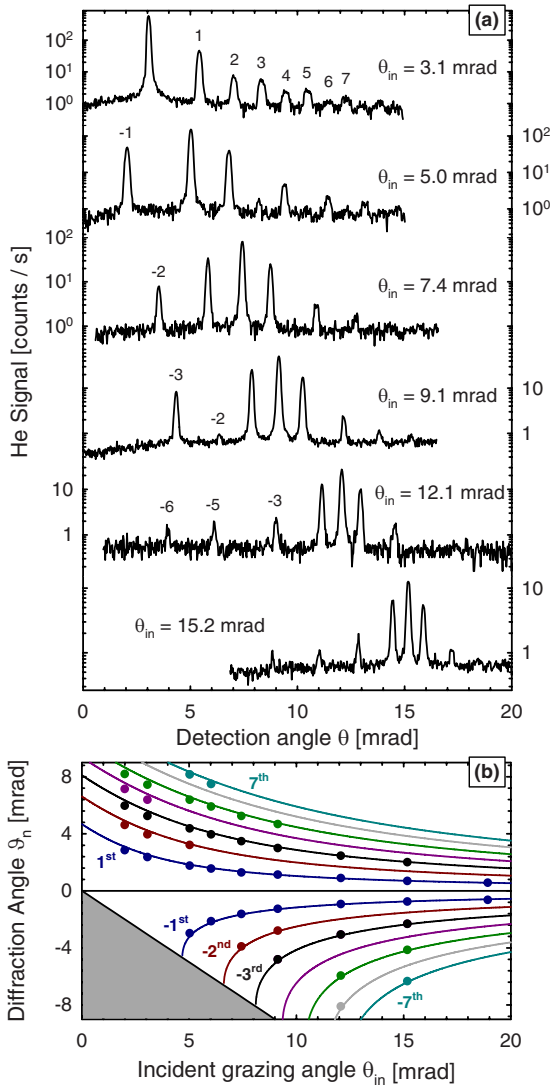

FIG. 2. (Color online) (a) Semilogarithmic plot of diffraction patterns observed for a He atom beam at $T_0=20$ K at various incident grazing angles as indicated. Numbers indicate the diffraction order assigned to the peaks. (b) Comparison between the observed diffraction angles and those calculated by the grating equation. The gray-shaded region indicates the regime beneath the surface given by $\vartheta_n<-\theta_{in}$.

minus-second-order peak which decreases sharply when θ_{in} is increased from 7.4 to 9.1 mrad.

To investigate the origin of these peak-height variations, we studied their dependence on the de Broglie wavelength by measuring two series of diffraction patterns at constant incident grazing angles of $\theta_{in}=4.9$ and 7.2 mrad (Fig. 3). In each series we varied the source temperature T_0 and, hence, the de Broglie wavelength, which is approximately proportional to $1/\sqrt{T_0}$ [20]. The broadening of peaks at small θ is readily understood from Fig. 2(b) where it can be seen that a small width of the incident θ_{in} distribution leads to an increased width in θ due to the steep slope of the lines close to the cutoff.

To quantify the observed diffraction peak-height variations we determine the relative diffraction intensities from the area under each diffraction peak divided by the area of

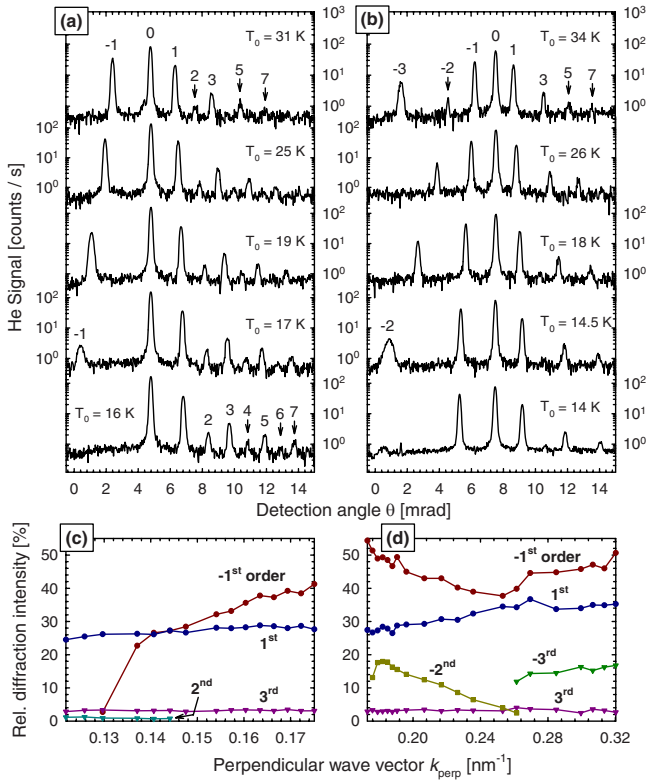

FIG. 3. (Color online) Diffraction patterns observed for He atom beams at various source temperatures for θ_{in}=4.9 (a) and 7.2 mrad (b). Numbers above the arrows indicate the diffraction order assigned to the peaks. Relative diffraction intensities, which are normalized to the zeroth-order intensity, are plotted for both series in (c) and (d), respectively, as a function of k_{perp}, the normal component of the incident wave vector. The relative error of these data points is around 10%.

the corresponding zeroth-order peak. In Figs. 3(c) and 3(d) the relative diffraction intensities are plotted as a function of $k_{perp} \approx \sin(\theta_{in})\sqrt{5k_B m T_0}/\hbar$, the normal component of the incident wave vector (with k_B the Boltzmann constant, m the particle mass, and $\hbar$ Planck's constant over 2π). The plots reveal (i) pronounced variations of the diffraction intensities with k_{perp} for some diffraction orders, (ii) even-order diffraction intensities up to 18%, and (iii) significant asymmetries between corresponding positive- and negative-diffraction-order intensities. None of the three observations can be explained by the Fraunhofer-Kirchhoff diffraction theory, which predicts the relative diffraction intensities for an amplitude grating to be independent of wavelength and to be determined by the ratio of grating period to strip width only [19]. As this ratio is 2 for our grating, the even-diffraction-order intensities are expected to vanish altogether. This behavior is indeed observed, but only in the limit of relatively large θ_{in} and θ, as can be seen in Fig. 2.

We therefore attribute our observations to the long-range atom-surface interactions which have been observed previously in experiments with nanoscale transmission gratings [6,7,21]. For the reflection grating the relative diffraction intensities are expected to be an even more sensitive probe of the atom-surface interaction than for a transmission grating,

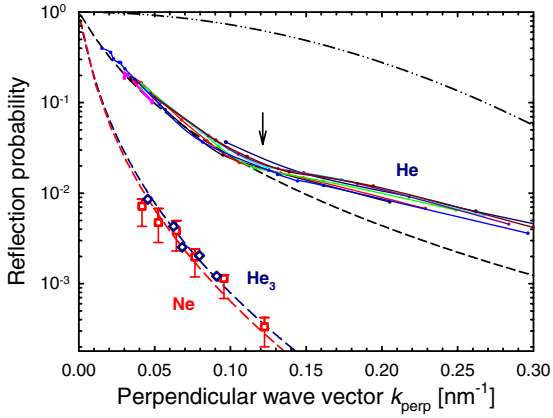

FIG. 4. (Color online) Observed coherent reflection probabilities for beams of He atoms [dots connected by solid lines, different lines correspond to different T_0 (6.7 to 20 K)], He trimers (open diamonds), and Ne atoms (open squares). The dash-dotted line presents a prediction for *classical reflection* from a hard-wall surface, tentatively assuming a roughness σ=4 nm. The dashed lines present predictions for *quantum reflection* at the long-range attractive branch of the surface potential. The kink is marked by an arrow.

because every part of the atomic wave function probes the interaction potential. In addition, for sufficiently small angles above the surface, the interaction path length is increased. A detailed theoretical model correctly accounting for the phase shift induced by the surface potential would be needed to determine the potential strength parameter from the data.

In Fig. 2 it can be seen that the peak heights decrease with increasing incident grazing angle. The total coherent reflection probability of the chromium strips is determined from the sum of all peaks normalized to the incident beam signal and multiplied by 2 to compensate for the 50% chromium coverage of the microstructure area. The reflection probability is as large as 40% at k_{perp}=0.015 nm^{-1} and decreases continuously to less than 1% at k_{perp}=0.3 nm^{-1} (Fig. 4). A kink at $k_{perp} \simeq 0.12$ nm^{-1} separates a steep decay at smaller k_{perp} from a slow simple exponential decay at larger k_{perp}. The dependence on k_{perp} differs significantly from what is expected for specular reflection of a wave from a randomly rough hard-wall surface at grazing incidence, which is given by $\exp[-(2\sigma k_{perp})^2]$, where σ denotes the root-mean-square roughness of the surface [22]. While this term does predict that even a rough surface reflects coherently in the limit $\sigma k_{perp} \to 0$, its dependence on k_{perp} exhibits the wrong curvature, as displayed by the dash-dotted line in Fig. 4.

A better agreement is obtained when we assume quantum reflection at the long-range attractive branch of the atom-surface potential to be the mechanism for coherent reflection. We calculate the quantum reflection probability by numerically solving the one-dimensional Schrödinger equation for an attractive Casimir–van der Waals surface potential of the approximate form $V(z)=-C_4/[(l+z)z^3]$. Here, z denotes the distance from the surface, and the coefficient $C_4=C_3 l$ is the product of the van der Waals coefficient C_3 and a characteristic length l (l=9.3 nm for He) indicating the transition from the van der Waals ($z \ll l$) to the Casimir regime ($z \gg l$) [13]. For small k_{perp} (left of the kink in Fig. 4) good agreement

with the data is found for $C_3=2.5\times10^{-50}$ J m^3. This value is slightly smaller than what is expected for He interacting with a transition metal surface [$(3.2-4.3)\times10^{-50}$ J m^3] but larger than what is expected for an insulating surface [23]. We attribute this behavior to an insulating chromium oxide surface having formed while the microstructure was exposed to air.

The kink and the slow decay at larger k_{perp} are not reproduced by this simple model. A similar kink was observed for He reflecting from a liquid He surface at $k_{perp}\simeq0.35$ nm^{-1} [24] and was explained by a quantum-reflection model based on a more realistic attractive potential shape [25]. As with increasing k_{perp} quantum reflection occurs at smaller z [13], the potential well region where the attractive branch deviates from a simple $-C_3/z^3$ power law starts to influence the quantum-reflection probability. Our calculations indicate that this effect can be neglected only as long as $k_{perp}<0.1$ nm^{-1}, where we find agreement with the calculation.

Further support for quantum reflection is given by the observation of reflected beams of He trimers and Ne atoms. For He trimers ($T_0=8.7$ K) the total coherent reflection probability increases by an order of magnitude to almost 10^{-2} when k_{perp} is lowered from 0.09 to 0.045 nm^{-1} (Fig. 4). The data are modeled very well with a C_3 coefficient three times that used for the He monomer calculation, as one would expect for a van der Waals–bound cluster of three He atoms. The binding energy of the He trimer is only 11 μeV [26]. Hence, it is more than three orders of magnitude smaller than the well depth of the estimated He_3-surface potential. As a result, classical reflection at the potential's repulsive inner branch should inevitably lead to dissociation.

For a Ne atom beam ($T_0=40$ K) the observed reflectivity data are well matched by the calculated quantum-reflection probability for $C_3=4.0\times10^{-50}$ J m^3 (dashed line in Fig. 4, characteristic length $l=11.84$ nm). As in the case of He this C_3 coefficient is again somewhat smaller than expected for a transition metal [$(7-9)\times10^{-50}$ J m^3 [23]].

In summary, we observed fully resolved diffraction peaks up to the seventh order for a He atom beam reflected from a 20-μm-period microstructured surface grating under grazing incidence. The observed relative diffraction intensities vary significantly with incident grazing angle and de Broglie wavelength. Furthermore, we observed coherent reflection probabilities from the surface grating for beams of Ne and of He_3 as a function of the normal component of the incident wave vector. The measurements are in excellent agreement with the predictions from a simple one-dimensional quantum-reflection model.

B.S.Z. acknowledges support by the Alexander von Humboldt Foundation and by the Korea Research Foundation Grant funded by the Korean Government (KRF-2005-214-C00188). We thank R. Brühl for assistance with the data-acquisition software and H. Conrad and J. R. Manson for fruitful discussions.

[1] *Atom Interferometry*, edited by P. R. Berman (Academic, New York, 1997).
[2] D. W. Keith, C. R. Ekstrom, Q. A. Turchette, and D. E. Pritchard, Phys. Rev. Lett. **66**, 2693 (1991).
[3] M. S. Chapman *et al.*, Phys. Rev. Lett. **74**, 4783 (1995).
[4] B. Brezger *et al.*, Phys. Rev. Lett. **88**, 100404 (2002).
[5] S. Gerlich *et al.*, Nat. Phys. **3**, 711 (2007).
[6] R. E. Grisenti, W. Schöllkopf, J. P. Toennies, G. C. Hegerfeldt, and T. Köhler, Phys. Rev. Lett. **83**, 1755 (1999).
[7] R. Brühl *et al.*, Europhys. Lett. **59**, 357 (2002).
[8] W. Schöllkopf and J. P. Toennies, Science **266**, 1345 (1994); J. Chem. Phys. **104**, 1155 (1996).
[9] F. Shimizu and J. I. Fujita, J. Phys. Soc. Jpn. **71**, 5 (2002).
[10] J. Grucker *et al.*, Eur. Phys. J. D **41**, 467 (2007).
[11] R. E. Grisenti *et al.*, Phys. Rev. A **61**, 033608 (2000).
[12] *Helium Atom Scattering from Surfaces*, edited by E. Hulpke *et al.* (Springer, Berlin, 1992).
[13] H. Friedrich, G. Jacoby, and C. G. Meister, Phys. Rev. A **65**, 032902 (2002).
[14] F. Shimizu, Phys. Rev. Lett. **86**, 987 (2001).
[15] H. Oberst, Y. Tashiro, K. Shimizu, and F. Shimizu, Phys. Rev. A **71**, 052901 (2005).
[16] T. A. Pasquini *et al.*, Phys. Rev. Lett. **97**, 093201 (2006).
[17] V. Druzhinina and M. DeKieviet, Phys. Rev. Lett. **91**, 193202 (2003).
[18] F. Shimizu and J. I. Fujita, Phys. Rev. Lett. **88**, 123201 (2002).
[19] M. Born and E. Wolf, *Principles of Optics* (Pergamon Press, London, 1959).
[20] *Atomic and Molecular Beam Methods*, edited by G. Scoles (Oxford University Press, Oxford, 1988).
[21] J. D. Perreault and A. D. Cronin, Phys. Rev. Lett. **95**, 133201 (2005).
[22] P. Beckmann and A. Spizzichino, *The Scattering of Electromagnetic Waves from Rough Surfaces* (Pergamon Press, London, 1963).
[23] G. Vidali *et al.*, Surf. Sci. Rep. **12**, 135 (1991).
[24] V. U. Nayak, D. O. Edwards, and N. Masuhara, Phys. Rev. Lett. **50**, 990 (1983).
[25] D. O. Edwards and P. P. Fatouros, Phys. Rev. B **17**, 2147 (1978).
[26] M. Lewerenz, J. Chem. Phys. **106**, 4596 (1997).